ChemComm

COMMUNICATION

View Article Online
View Journal | View Issue

Cite this: *Chem. Commun.*, 2022, **58**, 8081

Received 13th April 2022,
Accepted 20th June 2022

DOI: 10.1039/d2cc02114e

rsc.li/chemcomm

A chiral 3D silver(I)–benzenedithiolate coordination polymer exhibiting photoemission and non-linear optical response†

Saly Hawila,[a] Ahmad Abdallah,[a] Jean-Luc Rukemampunzi,[a] Alexandra Fateeva,[b] Gilles Ledoux,[c] Régis Debord,[c] Stéphane Paihlès,[c] Nathalie Guillou,[d] Florian Massuyeau,[e] Romain Gautier,[e] Adel Mesbah[a] and Aude Demessence *[af]

A new tridimensional metal–organic chalcogenolate, made of a 1, 3-benzenedithiolate bridging ligand and Ag(I), $[Ag_2(1,3\text{-BDT})]_n$, is reported. This coordination polymer has good thermal stability in air and displays both photoluminescence properties and a second harmonic generation response.

Metal–organic chalcogenolate (MOC) coordination polymers (CPs), made of ligands bearing chalcogen atoms (S, Se, and Te) as the coordinating functions, have received increasing attention for the formation of new networks and their intriguing electrical transport and photoluminescence properties.[1] Currently, most of the MOCs are made of coinage metals and thiolate ligands and the strong affinity between these soft acids and bases results in highly stable compounds. First, 1D and 2D MOCs have been reported with numerous functionalized monothiolate ligands and have shown great photoluminescence properties in the solid state,[2] such as the 1D $[Ag(o\text{-SPhCO}_2H)]_n$[3] that exhibits an intense orange emission or the 2D $[Cu(p\text{-SPhCO}_2Me)]_n$[4] that exhibits intrinsic triple emission bands associated with temperature-dependence for efficient ratiometric thermometry. Second, currently, copper and silver networks with a multithiolate ligand, benzenehexathiolate (BHT), exhibit the highest room temperature conductivity, among the CPs and metal–organic frameworks (MOFs), with 250 S cm^{-1} for the 3D structure of $[Ag_5(BHT)]_n$[5] and 1580 S cm^{-1} for the 2D $[Cu_3(BHT)]_n$.[6] Indeed, the metal–sulphur $(-M-S-)_n$ networks offer a good electrical conductivity, mainly due to the high overlap between the sulphur p-orbitals and the metal d-orbital and the electronic coupling between the conjugated organic and inorganic subunits. The recent chemical studies on $[Cu_x(BHT)]_n$ (x = 3, 4, and 5.5) and $[Ag_x(BHT)]_n$ (x = 3, 5) phases have shown the ability of the ligand to be oxidized with slightly different structures and electrical properties.[7] Since the report of these record conductivities with the BHT ligand, only two other d^{10} coinage MOC CPs have been reported with monothiolate ligands: $\{[Cu_2(6\text{-Hmna})(6\text{-mn})]\cdot NH_4\}_n$ (1, 6-Hmna = 6-mercaptonicotinic acid, 6-mn = 6-mercaptonicotinate)[8] exhibiting a 2D structure and an electrical conductivity of 11 S cm^{-1} and $[Ag(pyrine\text{–}2\text{-thiolate})]_n$, also 2D with 2×10^{-5} S cm^{-1} conductivity.[9] Thus, there is a tremendous need to develop new d^{10} coinage MOCs with other thiolate ligands in order to understand their structure–property relationships and control their band gaps to obtain either photoluminescent or conducting materials. Here we report the first d^{10} coinage MOC made of silver and a ditopic thiolate linker, the 1,3-benzenedithiolate (1,3-BDT) ligand, $[Ag_2(1,3\text{-BDT})]_n$. The compound crystallized in a chiral cubic structure that is discussed and its thermal stability is reported. This new MOC behaves as an insulator, but exhibits low temperature solid state photoemission and a second harmonic generation (SHG) response.

$[Ag_2(1,3\text{-BDT})]_n$ is synthesized by mixing silver nitrate and 1,3-benzenedithiol under hydrothermal conditions for 2 h at 120 °C. The pale-yellow powder was carefully washed with DMF to remove all the unreacted reagents especially the disulphide species formed as side products and that could remain in the amorphous form. The C, H, and S elemental analysis and thermogravimetric analysis (TGA) are in good accordance with the formulation of one ligand for two metals, which respects the charge balance (Fig. S1, ESI†). The infrared spectrum also confirms the presence of the coordinated benzenethiolate and the absence of thiol function usually observed at 2500 cm^{-1} (Fig. S2, ESI†). The images of the scanning and transmission

[a] *Université Lyon, Université Claude Bernard Lyon 1, Institut de Recherches sur la Catalyse et l'Environnement de Lyon (IRCELYON), UMR CNRS 5256, Villeurbanne, France. E-mail: aude.demessence@ircelyon.univ-lyon1.fr*
[b] *Université Lyon, Université Claude Bernard Lyon 1, Laboratoire des Multimatériaux et Interfaces (LMI), UMR CNRS 5615, Villeurbanne, France*
[c] *Université Lyon, Université Claude Bernard Lyon 1, Institut Lumière Matière (ILM), UMR CNRS 5306, Villeurbanne, France*
[d] *Université Paris-Saclay, UVSQ, Institut Lavoisier de Versailles (ILV), UMR CNRS 8180, Versailles, France*
[e] *Nantes Université, CNRS, Institut des Matériaux de Nantes Jean Rouxel (IMN), Nantes, France*
[f] *BCMaterials (Basque Center for Materials, Applications & Nanostructures), University of the Basque Country (UPV/EHU), Leioa, Spain*

† Electronic supplementary information (ESI) available: Syntheses, experimental setups, PXRD data, TGA, FT-IR, SEM, TEM, conductivity, photoluminescence and SHG details. CCDC 2164441. For ESI and crystallographic data in CIF or other electronic format see DOI: https://doi.org/10.1039/d2cc02114e

electron microscopies show that $[Ag_2(1,3\text{-BDT})]_n$ forms particles of around 100 nm with a cubic shape that can be observed with high resolution (Fig. S3, ESI†). The powder X-ray diffraction (PXRD) pattern collected at the CRISTAL beamline of the SOLEIL synchrotron facility (Gif-Sur-Yvette, France) shows high crystallinity of the compound and allows its *ab initio* structural determination. The final Rietveld refinement (Fig. S4, ESI†) leads to a satisfactory model indicator and profile factors (see Table S1, ESI†). $[Ag_2(1,3\text{-BDT})]_n$ crystallizes in the cubic chiral $P2_13$ space group with a = 12.88562(3) Å, V = 2139.52(1) Å^3 and Z = 12. The asymmetric unit contains four independent silver atoms with one (Ag1) in general position, and the three others (Ag2, Ag3, and Ag4) on the threefold axes, as well as one 1,3-BDT ligand ($C_6H_4S_2$) in general position. Each silver atom is coordinated to three sulphur atoms to form a near planar triangular geometry (Fig. 1b) with the Ag–S interatomic distances of 2.508(2) Å and 2.509(2) Å (Ag1–S1), 2.638(2) Å (Ag1–S2), 2.515(3) Å (Ag2–S1), 2.563 Å (Ag3–S2) and 2.618 Å (Ag4–S2). These distances are in total agreement with those found in the literature for this family of compounds such as in the case of the $[Ag(o\text{-SPhCO}_2H)]_n$ with Ag–S distances observed in the 2.487–2.639 Å range.[3] Simultaneously, each of the two independent sulphur atoms of the ligand is also coordinated to three silver atoms (Fig. 1a). The sulphur network is constructed from two independent empty octahedra, Ag_4S_6 (in blue on Fig. 1) and Ag_2S_6 (in cyan on Fig. 1), centred on the threefold axes and connected through sharing edges. Half of the faces of the first one, Ag_4S_6 (in blue), is occupied by three Ag1 and one Ag4, which are connected through sharing of sulphur corners and form a tetrahedron. Just two faces of the second octahedron, Ag_2S_6 (in cyan), are occupied by one Ag2 and one Ag4, connected through argentophilic interactions between them (3.0047(9) Å) (Fig. 1b). The empty capped Ag_4S_6 octahedra are then connected to three Ag_2S_6 ones by sharing edges and *vice versa*, to grow in the three directions and generate eight membered ring channels in the [111] direction filled by the organic moiety of the bridging 1,3-BDT ligands (Fig. 1e, f and Fig. S5–S7, ESI†). On the other hand, the silver network can be described from helical chains running along the *a* axis, in which coinage metals are bridged by sulphur atoms of the 1,3-BDT ligands following the Ag1–Ag4–Ag1–Ag3 sequence (Fig. 1g and Fig. S8, ESI†) and onto are grafted Ag2 by argentophilic interactions. Each helix is connected to four neighbouring ones through Ag1. Since this compound is cubic, these helices run also along the *b* and *c* axes, and intersect each other to generate this 3D chiral framework.

The TGA curve measured in air at a heating rate of 10 °C min^{-1} shows that $[Ag_2(1,3\text{-BDT})]_n$ is stable up to 400 °C (Fig. S1, ESI†). Thus, to study its thermal behaviour *ex situ* PRXD experiments have been first carried out. Five samples of $[Ag_2(1,3\text{-BDT})]_n$ have been calcined in an oven under an air atmosphere for one hour (ramp of 2 °C min^{-1}) at 200, 250, 300, 350 and 450 °C. Upon these calcinations the pale yellow powder turns progressively to dark brown up to 350 °C and becomes light grey at 450 °C (Fig. 2a). The Rietveld refinements (Table S2, ESI†) of the corresponding PXRD patterns show that $[Ag_2(1,3\text{-BDT})]_n$ is present at 100 wt% after calcination at 200 °C. Then, at 250 and 300 °C, the β-Ag_2S phase starts to be qualitatively observed, as it can be seen from the formation of darker powder, but its low quantity and small particle diameter prevent an accurate quantification. At 350 °C, 68 wt% of $[Ag_2(1,3\text{-BDT})]_n$ remains with 27 wt% of β-Ag_2S and 5 wt% of Ag. On the SEM images of these calcined samples, β-Ag_2S can be seen as around 1 μm aggregates and Ag (FCC) as micrometric crystals (Fig. S9, ESI†). Finally at 450 °C, there is no more $[Ag_2(1,3\text{-BDT})]_n$ but a mixture of 58 wt% of Ag and 42 wt% of Ag_2SO_4, probably because of the working conditions under the air atmosphere. These *ex situ* experiments show that $[Ag_2(1,3\text{-BDT})]_n$ has a complex decomposition process, starting from the formation

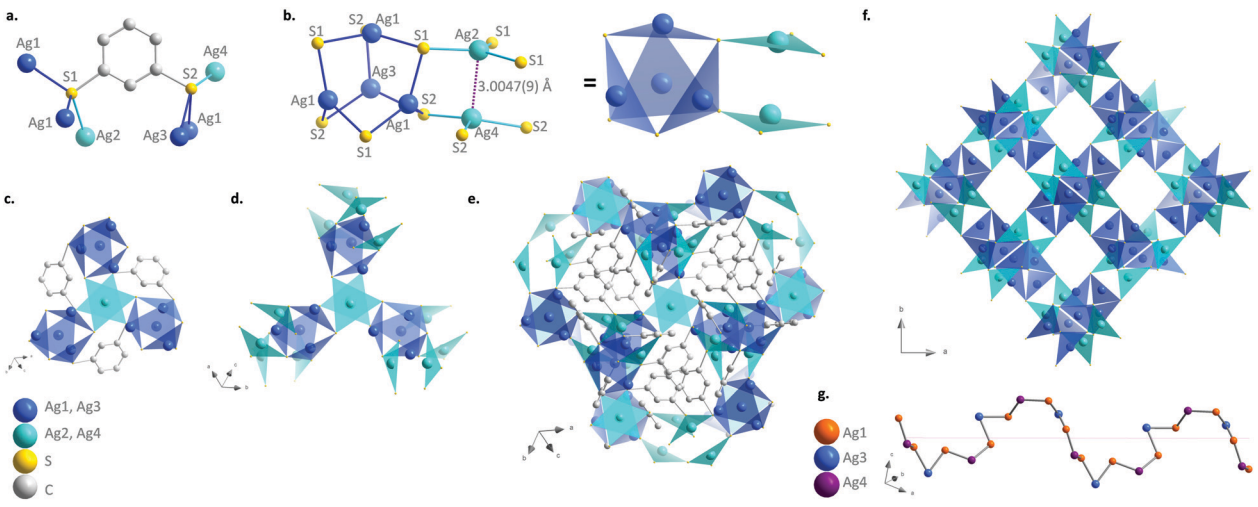

Fig. 1 Representations of the structure of $[Ag_2(1,3\text{-BDT})]_n$: (a) the ligand and its coordination to silver atoms; (b) the two sulphur-based octahedra: Ag_4S_6 (in blue) and Ag_2S_6 (in cyan); (c) the Ag_2S_6 octahedron (in cyan) connected to three Ag_4S_6 octahedra (in blue) with three bridging 1,3-benzenedithiolate ligands; (d) the same as (c) with the addition of two Ag_2S_6 octahedra connected to each Ag_4S_6 (ligands are not represented); (e) the same as (d) with the extension of the network and with the 1,3-benzenedithiolate ligands; (f) the network on the (*ab*) plane and without the ligand and (g) the chiral helix made of Ag1, Ag3 and Ag4.

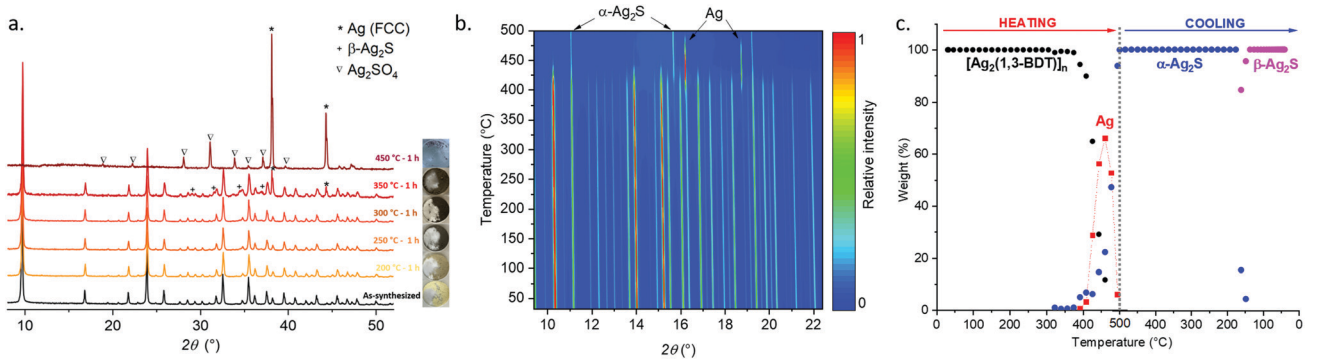

Fig. 2 (a) Normalized intensities of RT PXRD patterns (λ = 1.54056 Å) of *ex situ* calcinations of $[Ag_2(1,3\text{-BDT})]_n$ for one hour in air at 200, 250, 300, 350 and 450 °C. On the right, the photos of the sample after their calcinations. (b) 2D map of relative intensities of *in situ* PXRD (λ = 0.67122 Å) of $[Ag_2(1,3\text{-BDT})]_n$ with temperature from RT to 500 °C at 10 °C min^{-1} in air and (c) weight percentages of the different phases ($[Ag_2(1,3\text{-BDT})]_n$ (black), Ag (red), α-Ag_2S (blue) and β-Ag_2S (pink)) present upon heating and cooling.

of β-Ag_2S and followed by the formation of Ag and then, the emergence of Ag_2SO_4 (with no more β-Ag_2S) that is known to decompose at higher temperature into bulk Ag associated with the release of SO_2.[10] *In situ* temperature-dependent synchrotron PXRD experiments (on CRISTAL beamline, SOLEIL) have been carried out in a revolving open capillary under air flow and heated up to 500 °C at 10 °C min^{-1}. Fig. 2a and b show that under these dynamic conditions, $[Ag_2(1,3\text{-BDT})]_n$ remains the only phase up to 374 °C. Then from 392 °C, bulk silver starts to form, it reaches a maximum at 460 °C (66 wt%) and simultaneously with the CP decomposition, it is converted to α-Ag_2S (Fig. S10–S13, ESI†). At 500 °C, α-Ag_2S is the only phase and upon cooling its phase changes to β-Ag_2S that is observed at 161 °C and is the only phase at room temperature (Fig. S14, ESI†).[11] The comparison between these *ex* and *in situ* experiments shows that for the first one β-Ag_2S is a metastable phase and Ag_2SO_4/Ag is the residual mixture and for the second one Ag is the transition phase and the final product is β-Ag_2S. This points out the importance of the heating rate and time.

In order to measure the conductivity by the four-probe method, pellets pressed at 700 MPa have been fabricated with the as-synthesized $[Ag_2(1,3\text{-BDT})]_n$ and with the calcined samples for 1 h from 200 to 450 °C. The densities of the pellets are measured by the Archimedes' principle method. The mean value of the density of CP pressed at 700 MPa is 2.83 ± 0.23 g cm^{-3}. Knowing the density from the crystallographic data is 3.3 g cm^{-3}, the compactness of the pellets is around 86%. The PXRD patterns measured on the 4 mm diameter pellets and their quantitative analyses obtained from Rietveld refinements (Fig. S15 and Table S2, ESI†) show that under a pressure of 700 MPa, $[Ag_2(1,3\text{-BDT})]_n$ calcined up to 300 °C remains unaltered. $[Ag_2(1,3\text{-BDT})]_n$ is stable under a mechanical pressure of 700 MPa. The sample calcined at 350 °C, which has a mixture $[Ag_2(1,3\text{-BDT})]_n$/β-Ag_2S/Ag, is pressed at 700 MPa. The conductivity of the as-synthesized $[Ag_2(1,3\text{-BDT})]_n$ is about 10^{-10} S cm^{-1}, a very low value characteristic of insulators (Fig. S16, ESI†). The absence of conductivity can be related to the absence of the dithiolene motif as in the BHT linker, which permits better π-conjugation.[5] Then the conductivity increases slightly upon calcination of $[Ag_2(1,3\text{-BDT})]_n$ and reaches 10^{-7} S cm^{-1} for samples heated at 300 and 350 °C (Fig. S17, ESI†). On the other hand, the sample heated at 450 °C, where there is only bulk silver and Ag_2SO_4, exhibits a density of 8.34 g cm^{-3} and a conductivity of 7 × 10^{-5} S cm^{-1}. Thus, the increase of the conductivity of the samples calcined at 300 and 350 °C originates from the presence of the inorganic silver content. The absence of electrical conductivity in $[Ag_2(1,3\text{-BDT})]_n$ is mostly due to its wide optical band gap of 2.7 eV (Fig. S18, ESI†). Its reduction with a solution of lithium triethylborohydride ($LiEt_3BH$) was also attempted;[5] unfortunately, while $[Ag_2(1,3\text{-BDT})]_n$ turns green after 20 min with no apparent decomposition from the PXRD pattern, it still remains an insulator (Fig. S19, ESI†).

Due to the argentophilic interactions of 3.0 Å between Ag2 and Ag4 (Fig. 1), photoluminescence experiments have been carried out on the powder from room temperature to −180 °C (Fig. 3a and Fig. S20, ESI†). At room temperature (RT) and for λ_{ex} = 410 nm, it exhibits very low intensity emission at 525 and 650 nm, and then by lowering the temperature the red band becomes more intense and shifts to 610 nm, while the band at 525 nm remains as a shoulder. The origin of these two bands is most probably from a ligand-to-metal charge transfer (LMCT) for the one at 610 nm and from an intra-ligand charge transfer (ILCT) for the one at 525 nm, as can be observed from the emission spectrum of the free 1,3-H_2BDT ligand (Fig. S21, ESI†).[3,12]

As $[Ag_2(1,3\text{-BDT})]_n$ crystallizes in the chiral $P2_13$ space group, it potentially exhibits non-linear optical properties.[13] To confirm the acentric structure, second harmonic generation (SHG) measurements were performed with potassium dihydrogen phosphate (KDP) as the reference (Fig. 3b and Fig. S22, ESI†). The measurements performed on the $[Ag_2(1,3\text{-BDT})]_n$ powder sample at RT with λ = 800 nm show a response at 400 nm confirming the non-centrosymmetry. Compared to KDP, this SHG response is modest. Thus, $[Ag_2(1,3\text{-BDT})]_n$ is the first SHG-active MOC. In addition to this SHG signal, $[Ag_2(1,3\text{-BDT})]_n$ has an emission band centred at 525 nm when excited at 800 nm. This band is also observed as a shoulder under λ_{ex} = 410 nm and has been attributed to an ILCT (Fig. 3a). The

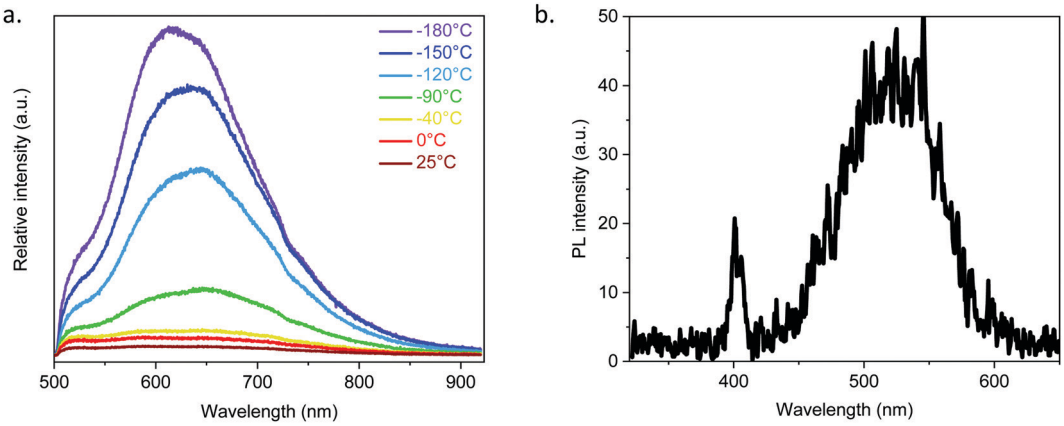

Fig. 3 Photophysical properties of $[Ag_2(1,3\text{-BDT})]_n$: (a) temperature-dependent solid state emission spectra (λ_{ex} = 410 nm) and (b) second harmonic generation response with incident beam at λ_{ex} = 800 nm and RT.

origin of the 525 nm emission band, when excited with low energy, can be due to energy transfer from the SHG signal or from an up-conversion mechanism. Further studies will be conducted to fully attribute this emission.

To conclude, we report a new neutral MOC made of a bidentate linker, 1,3-benzenedithiolate and Ag(I). Its 3D chiral cubic structure is made of the assembly of sulfur-based Ag_4S_6 and Ag_2S_6 octahedral motifs. More importantly, this CP has high thermal stability, up to 400 °C under dynamic air heating, and depending on the calcination conditions Ag_2S or Ag/Ag_2SO_4 can be obtained. Additionally, $[Ag_2(1,3\text{-BDT})]_n$ maintains its crystallinity under a pressure of 1 GPa. In terms of physical properties, while it is an insulating material, it exhibits a red-orange emission at low temperature and it is the first MOC exhibiting a SHG response associated with green emission at RT. This study confirms the great potential of the emerging MOCs in terms of physical properties. Thus, new MOCs with further thiolate-based ligands have to be discovered to rationalize the effects of π-conjugated organic moieties and the structure–property relationships, contributing to the development of highly stable functional materials on demand.

SH, AA and J-LR performed the synthetic experiments and routine characterization. AF performed the SEM imaging. GL carried out the photoluminescence experiments. RD and SP did the pellet formation and electrical analyses. NG and AM carried out the synchrotron experiments and PXRD analyses. FM and RG performed the SHG characterization. AD conceptualized the project, supervised and wrote the manuscript.

The authors acknowledge SOLEIL for provision of synchrotron radiation facilities and would like to thank Erik ELKAIM for assistance in using beamline CRISTAL. They also thank the CTμ for providing the SEM images, and the transport facilities for the electrical measurements and ILMTech for the sintering processes. This work was supported by the French National Agency (MEMOL ANR-16-JTIC-0004-01 and MOTIC ANR-21-CE08-0045). SH acknowledges the CNRS for her PhD grant and AA the Fondation de la Maison de la Chimie for his postdoctoral position. The European Commission is acknowledged by AD for her Marie Skłodowska-Curie Individual Fellowship (1010 31503—AniMOC—H2020-MSCA-IF-2020).

Conflicts of interest

There are no conflicts to declare.

References

1 Y. Kamakura and D. Tanaka, *Chem. Lett.*, 2021, **50**, 523.
2 (*a*) O. Veselska and A. Demessence, *Coord. Chem. Rev.*, 2018, **355**, 240; (*b*) Q. Wang, S.-L. Dong, D.-D. Tao, Z. Li and Y.-B. Jiang, *Coord. Chem. Rev.*, 2021, **432**, 213717.
3 O. Veselska, N. Guillou, M. Diaz-Lopez, P. Bordet, G. Ledoux, S. Lebègue, A. Mesbah, A. Fateeva and A. Demessence, *ChemPhotoChem*, 2022, e202200030.
4 O. Veselska, D. Podbevšek, G. Ledoux, A. Fateeva and A. Demessence, *Chem. Commun.*, 2017, **53**, 12225.
5 X. Huang, H. Li, Z. Tu, L. Liu, X. Wu, J. Chen, Y. Liang, Y. Zou, Y. Yi, J. Sun, W. Xu and D. Zhu, *J. Am. Chem. Soc.*, 2018, **140**, 15153.
6 X. Huang, P. Sheng, Z. Tu, F. Zhang, J. Wang, H. Geng, Y. Zou, C.-a Di, Y. Yi, Y. Sun, W. Xu and D. Zhu, *Nat. Commun.*, 2015, **6**, 7408.
7 (*a*) X. Huang, Y. Qiu, Y. Wang, L. Liu, X. Wu, Y. Liang, Y. Cui, Y. Sun, Y. Zou, J. Zhu, W. Fang, J. Sun, W. Xu and D. Zhu, *Angew. Chem., Int. Ed.*, 2020, **59**, 22602; (*b*) Y. Sun, X. Huang, Y. Jin, Y. Li, Z. Li, Y. Zou, Y. Sun and W. Xu, *Inorg. Chem.*, 2022, **61**, 5060; (*c*) Y. Jin, Y. Li, Y. Sun, M. Zhu, Z. Li, L. Liu, Y. Zou, C. Liu, Y. Sun and W. Xu, *J. Mater. Chem. C*, 2022, **10**, 2711.
8 A. Pathak, J.-W. Shen, M. Usman, L.-F. Wei, S. Mendiratta, Y.-S. Chang, B. Sainbileg, C.-M. Ngue, R.-S. Chen, M. Hayashi, T.-T. Luo, F.-R. Chen, K.-H. Chen, T.-W. Tseng, L.-C. Chen and K.-L. Lu, *Nat. Commun.*, 2019, **10**, 1721.
9 W. Su, M. Hong, J. Weng, R. Cao and S. Lu, *Angew. Chem., Int. Ed.*, 2000, **39**, 2911.
10 S. I. Sadovnikov and E. G. Vovkotrub, *J. Alloys Compd.*, 2018, **766**, 140.
11 (*a*) H. Schmalzried, *Prog. Solid State Chem.*, 1980, **13**, 119; (*b*) S. I. Sadovnikov, A. I. Gusev and A. A. Rempel, *Superlattices Microstruct.*, 2015, **83**, 35.
12 P. Ristić, T. R. Todorović, V. Blagojević, O. R. Klisurić, I. Marjanović, B. B. Holló, P. Vulić, M. Gulea, M. Donnard, M. Monge, M. Rodríguez-Castillo, J. M. López-De-Luzuriaga and N. R. Filipović, *Cryst. Growth Des.*, 2020, **20**, 4461.
13 N. Chen, M.-X. Li, P. Yang, X. He, M. Shao and S.-R. Zhu, *Cryst. Growth Des.*, 2013, **13**, 2650.

